第 33 卷第 5 期
2017 年 5 月

无 机 化 学 学 报
CHINESE JOURNAL OF INORGANIC CHEMISTRY

Vol.33 No.5
779-786

电化学自组装 Fe/Cu 纳米复合材料对铁镍电池高倍率及低温性能改性

刘 平[1] 朱 丁*,[2] 杨 军[1] 黄兰香[1] 陈云贵*,[1]

([1]四川大学材料科学与工程学院,成都 610065)

([2]四川大学新能源与低碳技术研究院,成都 610065)

摘要:通过在碱液中阴极还原铁酸铜(t-$CuFe_2O_4$)简便地实现了纳米 Fe/Cu 复合材料的自组装。采用循环伏安(CV)与 X 射线衍射(XRD)分析了自组装过程中的相变。通过透射电镜(TEM)、选区电子衍射(SAED)以及扫描透射–能谱分析(STEM-EDX)的表征可以发现电结晶得到的铁、铜纳米颗粒分布均匀且接触紧密。当用于铁镍电池负极时,Fe/Cu 纳米复合电极展现了较好的放电容量与充电接收能力,并具备优异的高倍率与低温性能。当电流密度高达 4 500 mA·g_{Fe}^{-1} 或运行温度仅为–40 ℃时,该电极仍拥有很好的输出容量与电位特性。线性扫描伏安(LSV)分析证明了该电极中原位生成的 Cu 纳米颗粒催化了活性 Fe 的阳极溶解动力学性能,因而明显改善了电极的高倍率与低温放电性能。

关键词:铁酸铜;自组装;纳米复合材料;铁电极;高倍率与低温性能

中图分类号:TB331 **文献标识码**:A **文章编号**:1001-4861(2017)05-0779-08

DOI:10.11862/CJIC.2017.089

Electrochemically Self-Assembled Fe/Cu Nanocomposite with Improved High-Rate and Low-Temperature Performances for Nickel-Iron Alkaline Battery

LIU Ping[1] ZHU Ding*,[2] YANG Jun[1] HUANG Lan-Xiang[1] CHEN Yun-Gui*,[1]

([1]*College of Materials Science and Engineering, Sichuan University, Chengdu* 610065, *China*)

([2]*Institute of New Energy and Low-Carbon Technology, Sichuan University, Chengdu* 610065, *China*)

Abstract: Fe/Cu nanocomposite was simply self-assembled through the cathodic decomposition of tetragonal spinel $CuFe_2O_4$ (t-$CuFe_2O_4$) in alkaline solution. The phase transition from t-$CuFe_2O_4$ to Cu/Fe_3O_4, and eventually to Fe/Cu composite was monitored by cyclic voltammetry (CV) and X-ray powder diffraction (XRD). Transmission electron microscope (TEM), selected area electron diffraction (SAED) and scanning TEM-energy dispersive X-ray (STEM-EDX) observations showed that the electro-crystallized copper and iron nanoparticles dispersed homogeneously and contacted intimately. When the Fe/Cu nanocomposite electrode was tested as the anode for nickel-iron (Ni-Fe) rechargeable battery, it exhibited enhanced discharge capacity, charge-acceptance and especially remarkable high-rate and low-temperature performances. Excellent capacity output and potential characteristics were achieved at high discharge current density (4 500 mA·g_{Fe}^{-1}) or low operation temperature (–40 ℃), respectively. Linear scanning voltammetry (LSV) analyses demonstrated that the incorporation of in situ formed copper facilitated the anodic kinetics of active iron, resulting to the markedly enhanced high-rate and low-temperature discharge-ability of electrode.

Keywords: copper ferrite; self-assembly; nanocomposite; iron alkaline electrode; high-rate and low temperature performance

收稿日期:2016-12-29。收修改稿日期:2017-03-11。

四川省科技支撑计划(No.2015GZ0133)资助项目。

*通信联系人。E-mail:ygchen60@aliyun.com,zhuding@scu.edu.cn,Tel:+86 13981815102,+86 13881955107

By virtue of its long service life, low cost, environmental friendliness, and excellent resistance to both physical and electrochemical abuse, Ni-Fe alkaline battery has been widely developed for traction, electric vehicles and stationary applications. Additionally, it may be a suitable substitution for lead-acid or nickel-cadmium battery as the large-scale energy storage system (>1 MW) in the view of environmental protection[1-2]. However, the bottlenecks of Fe anode, namely, extremely poor high-rate and low-temperature performances, low utilization of active iron and hydrogen evolution on the electrode lead to the decline in usage of Ni-Fe battery[3]. Over several decades of efforts, researchers have circumvented some of these problems to a substantial degree[4-20]. Various metal sulfides are demonstrated to markedly improve the capacity and the charge retention of Fe anode[4-9,15]. Hydrogen-oxygen recombinant catalyst is used to successfully suppress the gas evolution in battery[11]. And nanomaterial electrodes are confirmed to considerably enhance the utilization of active iron [10,17-18,20]. However, few investigations have simultaneously focused on the performances of Fe anode operated under extremely conditions, that is, low-temperature or high-rate. Since most of the present Fe alkaline electrodes are merely adapted to operation temperature above −15 ℃ and discharge current density below 300 $mA \cdot g_{Fe}^{-1}$ [3,5-6,8-16], significant improvements are urgently needed if we want to extend the application scope of Ni-Fe battery.

Slow anodic kinetics of active iron generally account for the poor low-temperature and high-rate performances of Fe alkaline electrode. The copper incorporation seems to be an effective way because Cu particles can effect as high conductive nucleation cores to greatly assist the anodic dissolution-deposition process of iron species. Recently, Kao and co-workers synthesized Fe/Cu nanocomposite via $NaBH_4$ reduction, which exhibited an outstanding capacity delivery at the current density up to 3200 $mA \cdot g_{Fe}^{-1}$ [20]. This study put forward an effective route to improve the poor rate performance of Fe anode, but the involved preparation are somewhat elaborate for practice, and the low-temperature performance and anodic kinetics of electrode are not referred.

In this study, a facile self-assembly of Fe/Cu nanocomposite through the cathodic decomposition of t-$CuFe_2O_4$ precursor is proposed. The electrochemical performances, especially the high-rate and low-temperature discharge-ability of Fe/Cu nanocomposite electrode are investigated in detail. In addition, LSV is employed to analyze the effect of copper incorporation on the anodic kinetics of iron.

1 Experimental

1.1 Syntheses of t-$CuFe_2O_4$

t-$CuFe_2O_4$ was prepared by a co-precipitation method[21]. Briefly, the aqueous solution of NaOH (5 $mol \cdot L^{-1}$) was added to the aqueous solution which contained 0.125 $mol \cdot L^{-1}$ $FeCl_3 \cdot 6H_2O$ and 0.062 5 $mol \cdot L^{-1}$ $CuCl_2 \cdot 2H_2O$. The as-formed brown suspension was stirred at 373 K for 2 h. Then the precipitate was filtered and washed with deionized water and alcohol, and dried at 373 K for 12 h. Finally, the precursor was calcined at 1 073 K for 2 h to form pure t-$CuFe_2O_4$ phase.

1.2 Self-assembly and characterization of Fe/Cu nano-composite electrode

Galvanostatic charging technique was used to induce the reduction of t-$CuFe_2O_4$ to self-assemble the Fe/Cu nano-composite electrode. The working electrode was fabricated by pasting a slurry mixture of 80% t-$CuFe_2O_4$, 15% acetylene black and 5% PVA onto a nickel foam (1 cm×1 cm) and then dried at 373 K for 12 h. Electrochemical experiments were performed using a three-electrode cell including one working electrode, four sintered $Ni(OH)_2$/NiOOH counter electrodes and one Hg/HgO reference electrode. The electrolyte comprised of 8 $mol \cdot L^{-1}$ KOH and 0.05 $mol \cdot L^{-1}$ Na_2S. The cathodic current density was kept at 300 $mA \cdot g_{oxide}^{-1}$ and the reduction time was 2 h.

The phase transition process was monitored by CV (Par2273 potentiostat with the potential range of 0 to −1.4 V at a sweep rate of 5 $mV \cdot s^{-1}$) and XRD (Dandong DX-2600 with Cu $K\alpha$ radiation, λ=0.154 18 nm, U=35 kV, I=25 mA, 2θ=20°~70°). TEM, SAED, STEM-EDX and high-resolution transmission electron

microscope (HRTEM) analyses were conducted on a Tecnai G220 S-TWIN microscope to observe morphology, elemental distribution and interface configuration of the as-formed Fe/Cu nanocomposite.

1.3 Electrochemical measurements of Fe/Cu nano-composite electrode

Galvanostatic discharging-charging tests were conducted to measure the electrochemical performances of Fe/Cu nanocomposite electrode. The capacity and charge-acceptance of Fe/Cu nanocomposite electrode were evaluated with a current density of 300 mA·g_{Fe}^{-1} under 30 ℃. To investigate the high-rate performance, the electrode was charged with a 300 mA·g_{Fe}^{-1} current density for 2 h, and the fully charged electrode was discharged at 50, 300, 1 500 and 4 500 mA·g_{Fe}^{-1} under 30 ℃, respectively. To investigate the low-temperature performance, the fully charged electrode was discharged under 30, 0, −20 and −40 ℃ at 50 mA·g_{Fe}^{-1}, respectively. The tests at lower temperatures were conducted after the system was held at a constant temperature for 2 h. LSV was employed to study the anodic kinetic properties of Fe/Cu nanocomposite electrode with various scan rates using the Par2273 potentiostat.

2 Results and discussion

2.1 Self-assembly of Fe/Cu nanocomposite electrode from t-$CuFe_2O_4$

Fig.1(a) illustrates the electrochemical redox behaviors of t-$CuFe_2O_4$ in aqueous alkaline solution. Four pairs of redox peaks appear in the CV curve of t-$CuFe_2O_4$. Referring to the CV curve of Fe_3O_4, two pairs of cathodic/anodic peaks Red_1/Ox_1 and Red_2/Ox_2 can be attributed to the reduction/oxidation of $Fe^{3+/2+}$ ⇌ Fe^{2+} and Fe^{2+} ⇌ Fe^0, respectively. The additional redox couples, marked as Red_1'/Ox_1' and Red_2'/Ox_2', correspond to the redox reactions of Cu^{2+} ⇌ Cu^+ and Cu^+ ⇌ Cu^0[22], respectively. Obviously, along the cathodic direction, copper cations are preferentially reduced to metallic state, then ferric iron is reduced to ferrous iron, and eventually to elemental iron. From a thermodynamics point of view, Cu can keep metallic state while Fe undergoes the reversibly faradic reactions (Fe^{3+} ⇌ Fe^0) in a certain potential range (the left area of the dot in Fig.(1a)).

Fig.1(b) records the phase transition during the self-assembly of Fe/Cu nanocomposite from t-$CuFe_2O_4$. Initially, only t-$CuFe_2O_4$ phase can be detected. Then t-$CuFe_2O_4$ decomposes into Cu/Fe_3O_4 composite after Red_2' reaction. Finally, magnetite converts into metallic Fe while Cu remains stable. The elemental Cu and Fe exist not as alloy or solid-solution but as two separated phases due to the immiscibility. The crystallite size of each phase is calculated to be 54.9 nm (Cu) and 61.8 nm (Fe) using the Scherrer equation, suggesting the self-assembly of Fe/Cu composite at the nanoscale.

TEM image also confirms the nano-level combination of iron and copper (Fig.2(a)). Indeed, the average particle size is below 100 nm and consistent with XRD results. SAED (Fig.2(a), Inset) presents a clear spots and rings pattern demonstrating the nanocrystalline nature. Judging from the d-spacing,

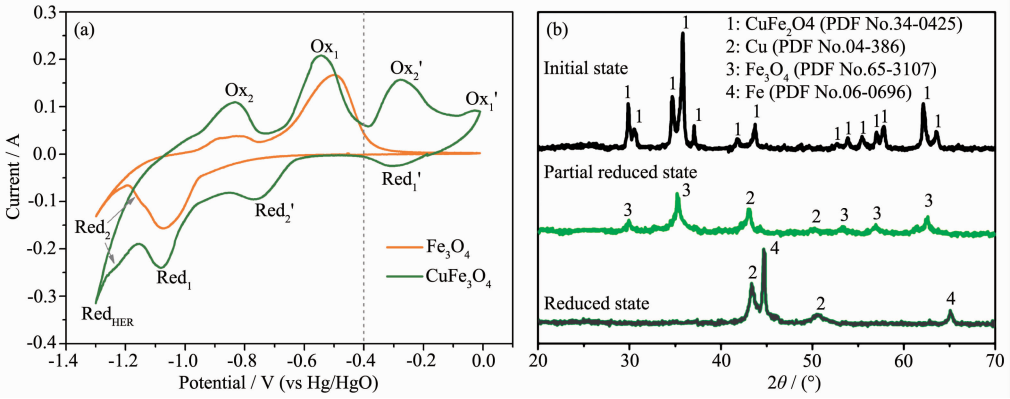

Fig.1 Self-assembly of Fe/Cu nanocomposite electrode from t-$CuFe_2O_4$: (a) Redox behavior of t-$CuFe_2O_4$ compared to Fe_3O_4; (b) Phase transition upon the self-assembly process

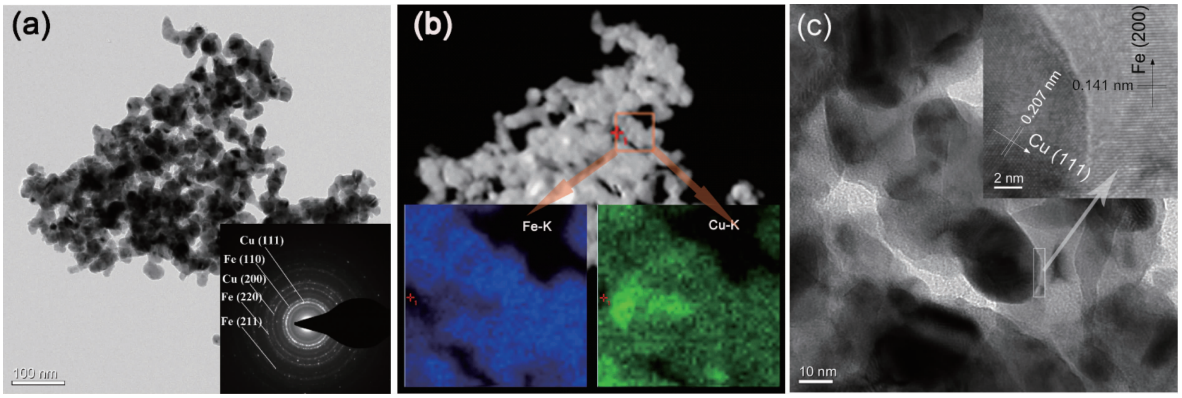

Inset: (a) SAED pattern taken at the same zone; (c) interface between Cu and Fe nanoparticles

Fig.2 Characterization of Fe/Cu nanocomposite electrode: (a) TEM overview; (b) STEM-EDX element mapping for Fe and Cu at a random area; (c) HRTEM image

the five distinct rings can be indexed to the (111) and (200) reflections of Cu, and to the (110), (220) and (221) reflections of Fe, respectively. Element mapping for either Fe or Cu (Fig.2(b)) reveals the homogeneous dispersion of two phases, which can be further proved by the HRTEM image (Fig.2(c)), where two kinds of nanoparticles with different contrasts distribute uniformly. The inset of Fig.2(c) gives more information about the crystal structure and the interface configuration of the nanocomposite. The lattice fringes illustrate the well crystallinity of two nanoparticles and exhibit the interplanar distances of 0.207 nm (the dark) and 0.141 nm (the light) that are characteristic of copper (111) planes and iron (200) planes, respectively, agreeing well with the analyses of XRD and SEAD. An intimate contact between two metallic grains is pronounced around the phase boundary.

Considering that the bonding nature of Cu-O is weaker than that of Fe-O in t-$CuFe_2O_4$[23], and that the equilibrium potentials of $Cu^{2+} \rightleftharpoons Cu^0$ reactions are more positive than those of $Fe^{3+} \rightleftharpoons Fe^0$ reactions, copper cations at the octahedral sites of t-$CuFe_2O_4$ are readily and preferentially reduced and migrated from the lattice upon the electrochemical reduction. Accompanied with the phase separation, the copper species dissolve and precipitate homogeneously on the surface of Fe species. The in situ formed Cu nanoparticles can uniformize the cathodic current distribution and suppress the coalescence of Fe grains to facilitate the electro-crystallization of Fe. Thus, Fe particles finely disperse and strongly contact within Cu nanoparticles to form the well-architectured Fe/Cu nano-composite.

2.2 Electrochemical performances of Fe/Cu nano-composite electrode

Fig.3 shows the typical charge-discharge profiles of Fe/Cu nanocomposite electrode, and the traditional Fe electrode is introduced for comparison. Both electrodes exhibit two pairs of potential plateaus, corresponding to Red_1/Ox_1 and Red_2/Ox_2 in Fig.1(a), respectively. Briefly, Red_1/Ox_1 involves the diffusion of protons between the solid lattices of Fe_3O_4 and $Fe(OH)_2$. Red_2/Ox_2 represents the cathodic electro-crystallization and the anodic dissolution of Fe, respectively. The extra plateau in both charging curves (dot line) links to the hydrogen evolution reaction (HER). For the traditional Fe electrode, the potential plateaus of Red_2 and HER tend to overlap, and a lot of charging

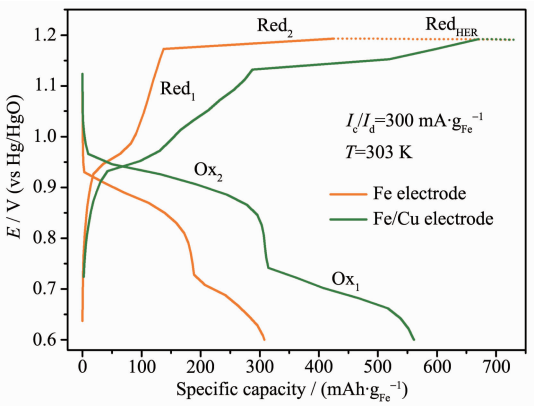

Fig.3 Typical charge-discharge profiles of Fe and Fe/Cu nano-composite electrodes

current is consumed to HER instead of Fe electrocrystallization, causing a poor charge-acceptance. On the other hand, Fe/Cu nanocomposite electrode shows a relatively low polarization of Red_2, thus Fe species can be mainly reduced before the electrolysis of water. Furthermore, both the discharge capacity and the potential characteristics of Fe/Cu electrode are markedly improved as compared to those of Fe electrode, suggesting that the incorporation of Cu enhances the utilization and anodic kinetics of active iron.

In the practical application of Fe alkaline electrode, only the Red_2/Ox_2 redox is involved[3]. So the following discussions on the high-rate and low-temperature discharge-ability mainly focus on the first discharge plateau. Fig.4 shows the comparison of the discharge curves for Fe and Fe/Cu electrodes at various current densities. Fe/Cu electrode displays a significantly enhanced high-rate performance than that of Fe electrode. When the current density increases from 50 to 1 500 mA·g_{Fe}^{-1}, the capacity retention of Fe/Cu electrode attains 72%, which is almost twice than that of Fe electrode (37%). When the current density further increases up to 4 500 mA·g_{Fe}^{-1}, Fe/Cu electrode still remains ~50% capacity output, whereas Fe electrode is close to failure. Besides, the potential plateau characteristics of Fe/Cu electrode under increased current density is also improved. The midpoint potential (E_{mid}) of Fe/Cu electrode at each current density is 0.94, 0.93, 0.9 and 0.83 V (vs Hg/HgO), respectively, and the corresponding value of Fe electrode is 0.91, 0.86, 0.78 and 0.7 V (vs Hg/HgO), respectively. Clearly, the anodic polarization of Ox_2 is significantly relieved for Fe/Cu nanocomposite electrode.

There are similar regulations between the influence of the low-temperature and the high-rate on the discharge-ability of Fe and Fe/Cu electrodes (Fig. 5). With the temperature decreasing from 30 to −40 ℃, both electrodes suffer capacity deterioration and increasing polarization. However, the temperature influence on the discharge-ability for Fe/Cu electrode is much smaller as compared to Fe electrode. At 30 ℃, the capacity and E_{mid} of Fe/Cu electrode are slightly higher than those Fe/Cu electrode, but the gaps between capacity and midpoint potential of two electrodes gradually widens with decreasing tempera-

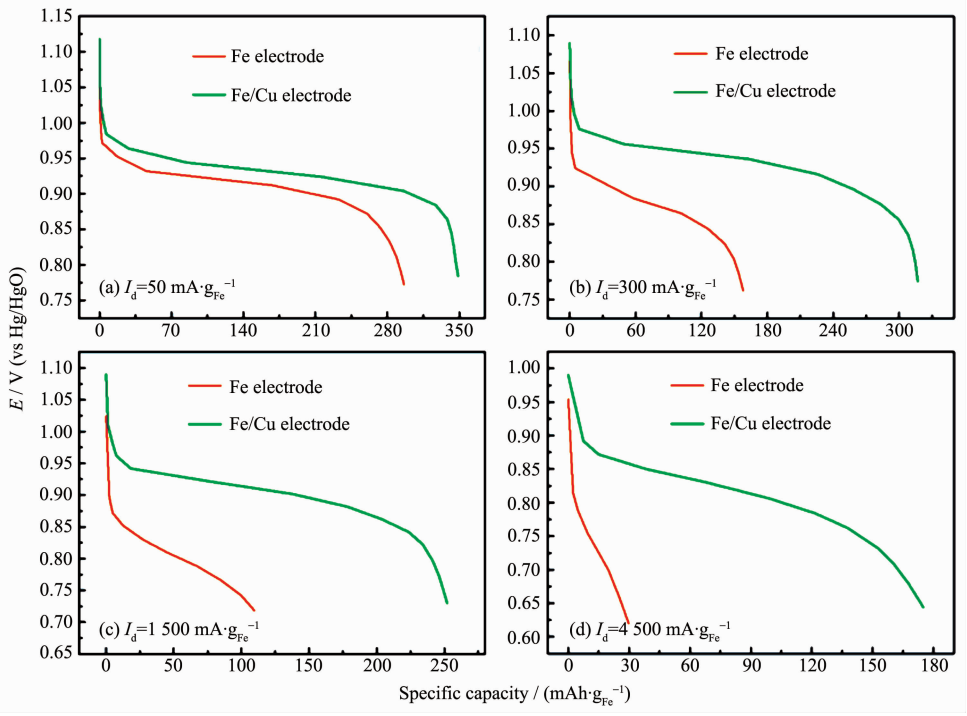

(a) 50 mA·g_{Fe}^{-1}, (b) 300 mA·g_{Fe}^{-1}, (c) 1 500 mA·g_{Fe}^{-1}, (d) 4 500 mA·g_{Fe}^{-1}

Fig.4　Discharge curves of Fe and Fe/Cu nanocomposite electrodes at various current densities

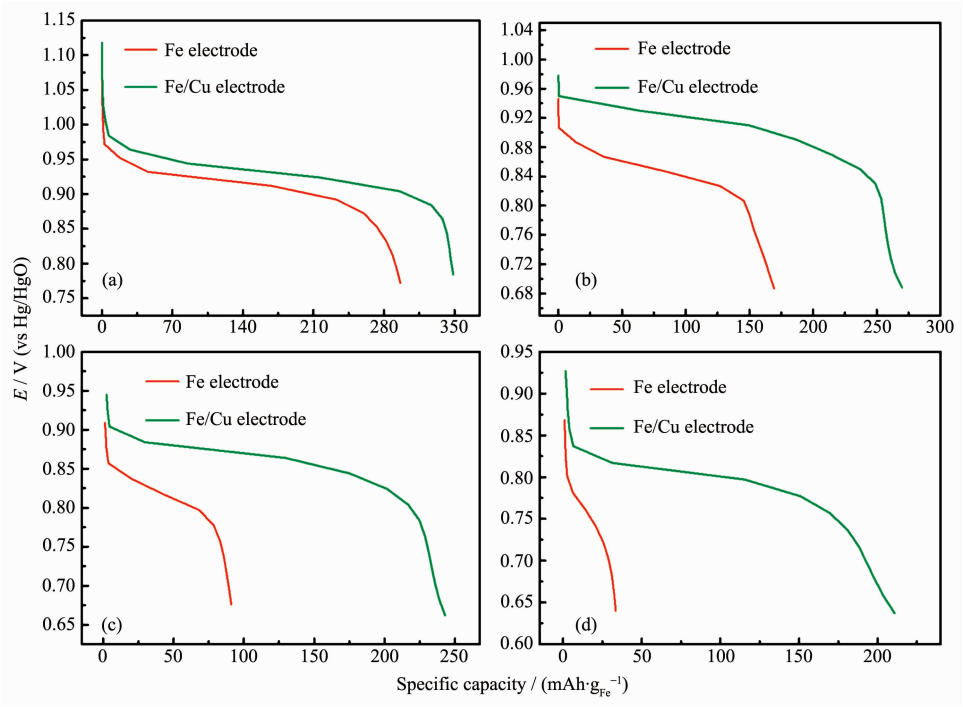

(a) 30 ℃, (b) 0 ℃, (c) −20 ℃, (d) −40 ℃

Fig.5 Discharge curves of Fe and Fe/Cu nanocomposite electrodes at various operating temperatures

ture. At −40 ℃, Fe/Cu electrode is able to deliver a capacity of 211 mAh·g_{Fe}^{-1}, which accounts for 61% of its capacity at room-temperature, and is more than seven times higher than the capacity output of Fe electrode (30 mAh·g_{Fe}^{-1}). Moreover, the E_{mid} value of Fe/Cu electrode is nearly 100 mV higher than that of Fe electrode at −40 ℃. It is clear that both the capacity output and the depolarization of the Fe/Cu nanocomposite electrode are significantly superior to those of the traditional Fe electrode in low-temperature environment. As previously stated, the copper species dissolve and precipitate homogeneously on the surface of Fe species. The in situ formed Cu nanoparticles can uniformize the cathodic current distribution and suppress the coalescence of Fe grains. Cu nanoparticles can also effect as high conductive nucleation cores to greatly promote the anodic dissolution-deposition process of Fe species, thereby significantly improve the performance of the electrode at low temperature.

2.3 Anodic kinetics of Fe/Cu nano-composite electrode

The excellent high-rate and low-temperature performances of Fe/Cu nanocomposite electrode can be attributed to the greatly enhanced anodic kinetics of Ox_2 reaction. To study the effect of Cu incorporation on the kinetics of Ox_2 reaction, LSV tests at various scan rates are conducted and the results are shown in Fig.6(a~b). Both the current response at each scan rate and the increment of current density with the scan rate are much higher for Fe/Cu electrode as opposed to Fe electrode. This implies that a much higher reaction rate of Ox_2 is achieved for Fe/Cu electrode. Furthermore, the shift in anodic peak potential is minimal for Fe/Cu electrode, indicating that Fe/Cu electrode suffers relatively low anodic polarization as previous discussion.

The variations of peak current density (I_p) with square root of the scan rate ($v^{1/2}$) for iron electrodes with and without Cu incorporation are plotted in Fig.7. The peak current densities of both electrodes varies linearly with the square root of scan rate. Such a linear relationship between I_p and $v^{1/2}$ for Ox_2 can be expressed as[24]:

$$I_p=Kv^{1/2} \quad (1)$$

Here K is the specific reaction rate constant for the

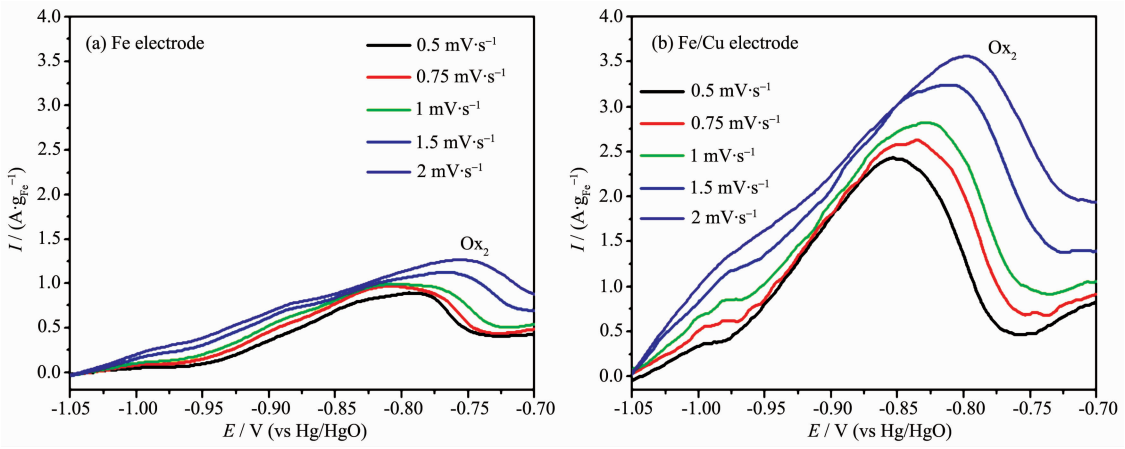

Fig.6　Anodic LSVs of Fe electrode (a) and Fe/Cu electrode (b) under various scan rates

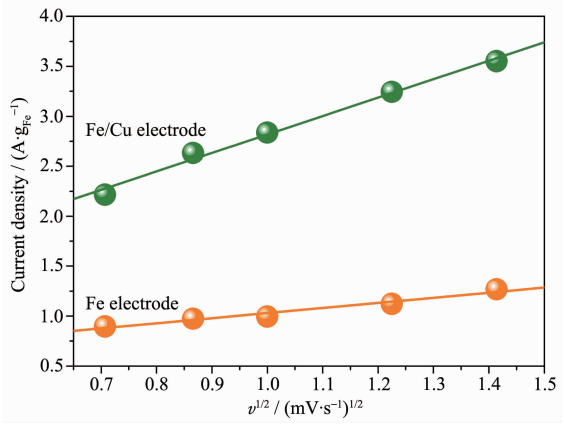

Fig.7　Relationship between I_p and $v^{1/2}$ for Fe and Fe/Cu nano-composite electrodes

metal dissolution reaction, which directly characterizes the reaction rate. Consequently, the kinetic properties of iron anodic dissolution can be largely evaluated from the slope of I_p to $v^{1/2}$ in Fig.7, and the Fe/Cu nanocomposite electrode evidently attains a much higher rate for Ox_2 reaction than Fe electrode.

The anodic reaction of iron electrode (Ox_2) can be represented as:

$$Fe+2OH^- \longrightarrow Fe(OH)_2+2e^- \quad (2)$$

It is a typical 'dissolution-deposition' process which proceeds through the following steps[25-26]:

$$Fe+OH^- \longrightarrow Fe(OH)_{ads}+e^- \quad (3)$$

$$Fe(OH)_{ads}+OH^- \longrightarrow [Fe(OH)_2]_{ads}+e^- \quad (4)$$

$$[Fe(OH)_2]_{ads}+OH^- \longrightarrow HFeO_2^-+H_2O \quad (5)$$

$$HFeO_2^-+H_2O \longrightarrow Fe(OH)_2+OH^- \quad (6)$$

For the traditional Fe electrode, the low solubility of intermediates ($HFeO_2^-$) is responsible for the extremely poor high-rate and low-temperature performances[3]. Due to the low solubility, $HFeO_2^-$ is prone to supersaturation before diffusing in the electrolyte, thereby the insoluble and insulating $Fe(OH)_2$ tends to precipitate at or near the anodic reaction site and block the active surface of Fe. In this study, the introduction of Cu significantly promotes the kinetics of Ox_2 reaction as is confirmed above. Since the Cu incorporation can hardly affect the solubility of $HFeO_2^-$ in the alkaline solution, it is reasonable to conclude that Cu nanoparticles play an important role in altering the passivation behavior of active iron. Presumably, these Cu particles of tight adhesion with active Fe phase act as the heterogeneous nucleation cores for $Fe(OH)_2$ deposition, which suppresses the cover of $Fe(OH)_2$ on the reaction sites upon discharge, and keeps the high effective interface between active Fe and electrolyte. Additionally, Cu nanoparticles of high electronic conductivity distributes homogeneously through the whole electrode, which constructs a high conductive network to guarantee the electrons transport when electrode suffers a severely passivation, significantly reducing the anodic polarization of electrode upon discharge.

3　Conclusions

In summary, a facile self-assembly of Fe/Cu nanocomposite from the cathodic decomposition of t-$CuFe_2O_4$ is presented. The electro-crystallized copper and iron nanoparticles disperse homogeneously and

contact intimately. When the as-prepared Fe/Cu nanocomposite electrode was tested as the anode for Ni-Fe alkaline battery, it exhibits enhanced discharge capacity, charge-acceptance and especially remarkable high-rate and low-temperature performances. Excellent capacity output and potential plateau characteristics can be achieved even at 4 500 $mA \cdot g_{Fe}^{-1}$ or −40 ℃. It is demonstrated that the incorporation of copper promotes the anodic kinetics of active iron upon the dissolution-deposition process, resulting to the greatly enhanced high-rate and low-temperature discharge-ability of the electrode.

The presented route still has room for optimization. Our further work shows that by adjusting the atomic ratio n_{Cu}/n_{Fe} in the pristine binary oxide can make the electrode to output much higher capacity while remaining the excellent rate performance (unpublished). The employment of other reductive methods, such as pulse charging or H_2 reduction, may assist the Fe/Cu composite to get more ideal morphology for practice. Furthermore, such route also has a promising application in Fe-air and Fe-AgO rechargeable alkaline batteries, which are bothered by the poor high-rate and low-temperature performances of Fe alkaline anodes as well.

References:

[1] Shukla A K, Venugopalan S, Hariprakash B. *J. Power Sources*, **2001**,**100**:125-148

[2] Ibrahim H, Ilinca A, Perron J. *Renewable Sustainable Energy Rev.*, **2008**,**12**:1221-1250

[3] Brodd R J, Linden D, Reddy T B. *Handbook of Batteries*. 3*rd Ed*. New York: McGraw-Hill, **2002**:25-45

[4] Kalaignan G P, Muralidharan V S, Vasu K I. *J. Appl. Electrochem.*, **1987**,**17**:1083-1092

[5] Ravikumar M K, Balasubramanian T S, Shukla A K. *J. Power Sources*, **1995**,**56**:209-212

[6] Periasamy P, Bahu B R, Iyer S V. *J. Power Sources*, **1996**, **62**:9-14

[7] Ravikumar M K, Balasubramanian T S, Shukla A K, et al. *J. Appl. Electrochem.*, **1996**,**26**:1111-1115

[8] Caldas C A, Lopes M C, Carlos I A. *J. Power Sources*, **1998**, **74**:108-112

[9] Souza C A C, Carlos I A, Lopes M C, et al. *J. Power Sources*, **2004**,**132**:288-290

[10]Wang Y D, Ai X P, Cao Y L, et al. *Electrochem. Commun.*, **2004**,**6**:780-784

[11]Hariprakash B, Martha S K, Hegde M S, et al. *J. Appl. Electrochem.*, **2005**,**35**:27-32

[12]Hang B T, Watanabe T, Eashira M, et al. *J. Power Sources*, **2005**,**150**:261-271

[13]Casellato U, Comisso N, Mengoli G. *Electrochim. Acta*, **2006**, **51**:5669-5681

[14]Ujimine K, Tsutsumi A. *J. Power Sources*, **2006**,**160**:1431-1435

[15]Hang B T, Yoon S H, Okada S, et al. *J. Power Sources*, **2007**,**168**:522-532

[16]Hang B T, Hayashi H, Yoon S H, et al. *J. Power Sources*, **2008**,**178**:393-401

[17]Huang K C, Chou K S. *Electrochem. Commun.*, **2007**,**9**:1907-1912

[18]Kao C Y, Chou K S. *J. Power Sources*, **2010**,**195**:2399-2404

[19]Urbaniak J, Skowroński J M, Olejnik B. *J. Solid State Electrochem.*, **2010**,**14**:1629-1635

[20]Kao C Y, Tsai Y R, Chou K S. *J. Power Sources*, **2011**,**196**: 5746-5750

[21]Shin H C, Choi S C. *Chem. Mater.*, **2001**,**13**:1238-1242

[22]Cudennec Y, Lecerf A, Gérault Y. *Eur. J. Solid State Inorg. Chem.*, **1995**,**32**:1013-1018

[23]Kameoka S, Tanabe T, Tsai A P. *Appl. Catal. A*, **2010**,**375**: 163-171

[24]Bard A J, Faulkner L R. *Electrochemical Methods*: *Fundamental and Applications*. New York: John Wiley & Sons. Inc., **1980**:6-20

[25]Shoesmith D W, Taylor P, Bailey M G, et al. *Electrochim. Acta*, **1978**,**23**:903-916

[26]Asakura S, Nobe K. *J. Electrochem. Soc.*, **1991**,**118**:13-18